THE USE OF A LINEAR QUARTER-CAR MODEL TO OPTIMIZE THE DAMPING IN A PASSIVE AUTOMOTIVE SUSPENSION SYSTEM – A FOLLOW-ON FROM MANY AUTHORS' WORKS OF THE RECENT 40 YEARS

ZBIGNIEW LOZIA[1]

Warsaw University of Technology

Summary

In this study, over 40-year achievements of many foreign and Polish authors in the field of methods of optimizing the characteristics of automotive suspension systems have been used. A method of conducting the optimizing calculations, further developed by the author, has been presented and exemplified by calculations of viscous damping in the passive suspension system of a vehicle moving on an uneven road surface with a random profile. To determine the discomfort and safety hazard measures, a linear quarter-car model of the suspension system and the spectral transmittance analysis method were employed. The results have been shown in the form of a dimensionless objective function, which was taken as a criterion of optimization in respect of ride comfort and safety. The limitation of deflections of the suspension system has been taken into account, too. The graphic form of this function, whose argument is the dimensionless suspension damping coefficient, resembles the pictorial qualitative relationships, shown in many publications by other authors and facilitating the interpretation of final results of the optimization.

Keywords: optimization, automotive suspension system, quarter-car model, damping in the suspension system

[1] Warsaw University of Technology, Faculty of Transport, ul. Koszykowa 75, 00-662 Warszawa, Poland, e-mail: lozia@wt.pw.edu.pl

1. Introduction

Two major research trends can be discerned in the field of motor vehicle dynamics. The first one deals with vertical movements of vehicle components (i.e. vehicle ride) and it is chiefly focused on the translational and angular vibrations in the vertical plane parallel or perpendicular to the vehicle symmetry plane. The other one is dedicated to the research on vehicle movements in the plane parallel to the road surface and covers the steerability and directional stability of vehicle motion with the driver's impact being taken into account (in general, this is referred to as vehicle handling). At present, both of these issues are described jointly, with the use of complex simulation models [15, 17]. For many years, however, they were treated separately, which was justified by the will to avoid models that would be too difficult for analysis [3]. This was connected with gradual development of the methods and tools for the research on motor vehicle dynamics. This history was described in brief by Croll in publication [3], where he referred to Segel's conference speeches and publications supported by The Institution of Mechanical Engineers. It was as late as in 1950s that mathematical methods began to be used, thanks to which analytical deliberations with limited computational potential became possible. The introduction of computer-based techniques and new methods of examining linear and non-linear mechanical systems with deterministic or random excitation has made it possible to carry out calculations that would be more extensive, with simple or more complex mathematical models being used. Particularly important here are monograph-like works, which provide a basis for building models with different complexity degree and for analysing their properties. For the authors from Western Europe and North America, this chiefly applies to the works by Meirovitch [16], Newland [20], Mitschke [17, 18], and Wong [32]. In Poland, considerable importance is also attached, apart from the above, to the works by Rotenberg [25], Kamiński and Pokorski [9], Osiecki [21, 22, 23], and Kasprzyk and Prochowski [10, 11].

The first publications backed up with extensive computer calculation results appeared as recently as in 1970s. Such works have been continued until now and they cover a wide spectrum of issues related to motor vehicle dynamics.

In this study, over 40-year achievements of many foreign and Polish authors in the field of methods of optimizing the characteristics of automotive suspension systems will be summed up. The optimization of linear damping in the suspension system of a vehicle moving on an uneven road surface with a random profile will be described here in detail.

2. Review of the literature concerning the quarter-car model and its applications in the field of optimizing the characteristics of automotive suspension systems

The quarter-car model (see Fig. 2) is a system with two degrees of freedom (2DOF), describing the vertical vibrations of a part of the vehicle body solid ("sprung mass") situated over one road wheel (here: one of four vehicle wheels) and vibrations of the masses connected with the road wheel ("unsprung mass"). The two mass elements are

connected with each other by a spring-damper system acting in parallel and representing the spring-damping properties of the suspension system of the specific wheel. The unsprung mass interacts with the ground through a spring-damper or spring-only element, which represents the spring-damping or spring-only properties of the road wheel in the radial direction. Sometimes the model shown in Fig. 2 represents a "half-car" instead of a "quarter-car". Its structure is identical but the system parameter values are doubled. Models with a structure as described above appeared in 1970s (see e.g. publications [10, 17, 25, 26]) and they were employed in many publications of 1980s (e.g. [9, 14, 18, 28, 29]) and 1990s (e.g. [4, 11, 19]). They are still useful in the 21st century for more complex and more extensive analyses, including the works that synthesize research results in the form of recommendations for vehicle designers (e.g. [5, 6, 12, 24, 27, 30, 31, 32]). They are both linear and non-linear models used for analyses of passive, semi-active, and active suspension systems. In some of the works, the model analyses are supplemented with experimental examinations of the systems whose structure is similar to that of the quarter-car model [12, 24, 30].

In the 21st century, the quarter-car model is used in sophisticated optimization algorithms, where Pareto-optimal solutions are sought at the assessment of designs of variable-damping, semi-active, and active suspension systems (e.g. [3, 4, 5, 6, 27, 28, 29, 30, 31, 32]), with random nature of selected model parameters (sprung mass determined by hardly-predictable vehicle load and tyre stiffness depending on inflation pressure, e.g. [5]) being taken into account.

The authors of an overwhelming majority of the publications where the said optimization problem is addressed enumerate three main assessment criteria, which are related to the minimization of the driver and passengers' discomfort measures as well as to changes in the normal reaction at the tyre/road contact and to reduction in the range of working displacements of the suspension system [3, 4, 5, 6, 10, 11, 17, 18, 19, 25, 26, 27, 28, 29, 30, 31, 32]. In publication [28], the previous works (carried out by 1987) on the influence of viscous damping in the suspension system on discomfort and safety hazard measures (changes in the radial force in the tyre) have been summed up. A contradiction between the existing requirements has been highlighted (this issue has been depicted in publications [24, 30]) – see e.g. Fig. 1, where the author has marked, as an example, a subjectively chosen damping level. The graph in Fig. 1 is a pictorial drawing and it is used in practice to perform such a function. Its content, however, is so evocative that the author of this study will strive to express the optimization criteria in a form similar to that of Fig. 1, but with employing measurable criteria of assessment. Increased viscous damping in the suspension system impairs the comfort but improves the safety. Doubts are aroused by the values of the comfort and safety measures corresponding to very low and very high damping: they suggest that very low damping results in the greatest comfort and that very high damping translates into a very high safety level. The author of this study has recognized that these fragments of the pictorial curves of Fig. 1 should be verified within the computation work. The results presented in the publications referred to above also show that a growth in the viscous damping is accompanied by a reduction in the range of working displacements of the suspension system.

Most of the authors of the publications quoted here assume that the excitation is a Gaussian stationary random process in the domain of wavelength L [m], wave number 1/L [1/m], or angular frequency of the longitudinal road profile $\Omega = 2\pi/L$ [rad/m]. The wavelength ranges taken by them into consideration are: 0.26-66.8 m [25], 0.1-100 m [28], or 0.3-100 m [17, 18]. The smoothing properties of vehicle tyres are also taken into account [2, 3, 14, 15]. The vehicle speed range for which the processes are analysed is even as wide as 10-50 m/s (36-180 km/h) [6]. In result of the selection of the range of road roughness wavelength and vehicle speed, the frequency band of the vibrations of model solids is determined. However, the said frequency band is also limited in consideration of the properties of the object under test or the problem being analysed (ride comfort, wheel/road interaction, etc.). In the publications quoted, the following frequency bands were chosen:

- from 0-8 Hz to 0-14 Hz [26];
- 0.25-15 Hz [29];
- 0-20 Hz [19, 31];
- 0-25 Hz or 0-30 Hz [17, 18, 30];
- 0-50 Hz or 1-60 Hz [32];
- 1-80 Hz [30];
- 0-90 Hz or even 0.8-150 Hz [25];
- 0.1-100 Hz [27].

A considerable limitation of the analyses carried out for frequencies of up to 80 Hz arises from the occurrence of phenomena related to the resonance of tyre structure; due to such phenomena, the simple model of spring characteristics of the tyre is inapplicable [28]. It is also important that the acceptability limits regarding the comfort of vibrations are specified in the ISO standards for a frequency band of 0-80 Hz [7].
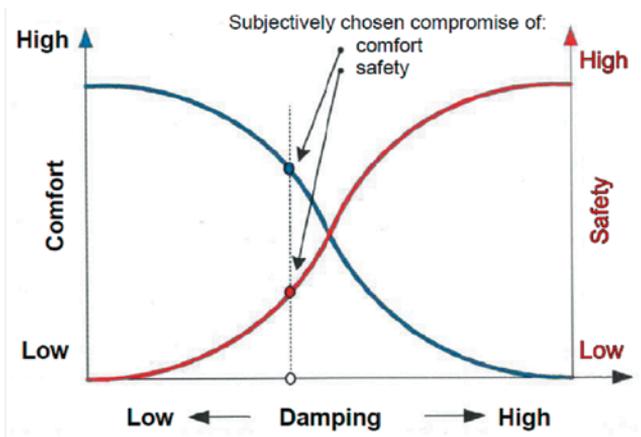
Fig. 1. Pictorial illustration of seeking a compromise between the comfort and safety requirements at the selection of constant damping in the suspension system [30]

3. Objective

The objective of this study is to present the methods of optimizing the characteristics of a passive automotive suspension system. A linear quarter-car model and an example procedure of determining the suspension damping coefficient will be described. The study will sum up the experience of the authors of the publications referred to herein, with introducing easier geometrical interpretations of the optimum values.

The calculation methods adopted have a wider range of applicability; as an example, they are particularly useful for determining the optimum values of the other parameters of the model under analysis.

4. The quarter-car model and its equations of motion in the time and frequency domain

Fig. 2 shows a physical representation of the quarter-car model. The model consists of two mass elements, i.e. a "sprung mass" with a mass of m_1 [kg] and an "unsprung mass" with a mass of m_2 [kg]. The suspension stiffness and the radial stiffness of the road wheel (pneumatic tyre) have been denoted by k_1 [N/m] and k_2 [N/m], respectively. The symbols c_1 [N·s/m] and c_2 [N·s/m] have the meaning of the coefficient of viscous damping of the suspension system and the coefficient of viscous damping representing the equivalent radial damping properties of the pneumatic tyre, respectively. The symbol ζ (t) represents the time-dependent kinematic excitation from an uneven road surface. The motor vehicle, as well as the model under consideration, moves rectilinearly with a constant speed V [km/h] (or v [m/s]).
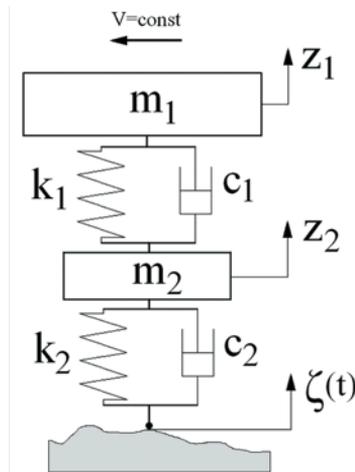
Fig. 2. Quarter-car model (for the notation used, see the text)

The equations of motion may be derived from the principles of dynamic force analysis, with taking into account the forces of inertia of the mass elements of the model. They have the form as presented in relation (1):

$$\begin{cases} m_1 \cdot \ddot{z}_1 + c_1 \cdot \dot{z}_1 + k_1 \cdot z_1 - c_1 \cdot \dot{z}_2 - k_1 \cdot z_2 = 0 \\ m_2 \cdot \ddot{z}_2 + (c_1 + c_2) \cdot \dot{z}_2 + (k_1 + k_2) \cdot z_2 - c_1 \cdot \dot{z}_1 - k_1 \cdot z_1 = c_2 \cdot \dot{\zeta} + k_2 \cdot \zeta \end{cases} \tag{1}$$

Their matrix form is shown in relation (2), where the symbols of the matrices of inertia $\mathbf{M}$, viscous damping $\mathbf{C}$, stiffness $\mathbf{K}$, excitation influences transmitted by the damping in the pneumatic tyre $\mathbf{C}_\zeta$, and excitation influences transmitted by the radial stiffness of the pneumatic tyre $\mathbf{K}_\zeta$ have been indicated. The vectors of the generalized coordinates (displacements), velocities, and accelerations have been denoted by $\mathbf{q}, \dot{\mathbf{q}}, \ddot{\mathbf{q}}$, respectively. This notation has been adopted in relation (equation) (3), which is the most concise form of presenting the relation (1).

$$\underbrace{\begin{bmatrix} m_1 & 0 \\ 0 & m_2 \end{bmatrix}}_{\mathbf{M}} \cdot \underbrace{\begin{bmatrix} \ddot{z}_1 \\ \ddot{z}_2 \end{bmatrix}}_{\ddot{\mathbf{q}}} + \underbrace{\begin{bmatrix} c_1 & -c_1 \\ -c_1 & c_1 + c_2 \end{bmatrix}}_{\mathbf{C}} \cdot \underbrace{\begin{bmatrix} \dot{z}_1 \\ \dot{z}_2 \end{bmatrix}}_{\dot{\mathbf{q}}} + \underbrace{\begin{bmatrix} k_1 & -k_1 \\ -k_1 & k_1 + k_2 \end{bmatrix}}_{\mathbf{K}} \cdot \underbrace{\begin{bmatrix} z_1 \\ z_2 \end{bmatrix}}_{\mathbf{q}} = \underbrace{\begin{bmatrix} 0 \\ c_2 \end{bmatrix}}_{\mathbf{C}_\zeta} \cdot \dot{\zeta} + \underbrace{\begin{bmatrix} 0 \\ k_2 \end{bmatrix}}_{\mathbf{K}_\zeta} \cdot \zeta \tag{2}$$

$$\mathbf{M} \cdot \ddot{q} + \mathbf{C} \cdot \dot{q} + \mathbf{K} \cdot q = \mathbf{C}_\zeta \cdot \dot{\zeta} + \mathbf{K}_\zeta \cdot \zeta \tag{3}$$

For equation (3), the Laplace transform has been formulated and, after transformations, equation (4) has been obtained, where the domain $s = r + i \cdot \omega$ has a real part r and an imaginary part ω, while $i_2 = -1$ (ω is the radian frequency [rad/s]):

$$(\mathbf{M} \cdot s^2 + \mathbf{C} \cdot s + \mathbf{K}) \cdot q(s) = (\mathbf{C}_\zeta \cdot s + \mathbf{K}_\zeta) \cdot \zeta(s) \tag{4}$$

The solution of this equation has the form (5):

$$q(s) = (\mathbf{M} \cdot s^2 + \mathbf{C} \cdot s + \mathbf{K})^{-1} \cdot (\mathbf{C}_\zeta \cdot s + \mathbf{K}_\zeta) \cdot \zeta(s) \tag{5}$$

The operational transmittance (transfer function) for displacements (6) is the ratio of the Laplace transform of the output signal (response) of a system to the input signal (excitation) of the same system at zero initial conditions:

$$H_q(s) = \begin{bmatrix} H_{q_1}(s) \\ H_{q_2}(s) \end{bmatrix} = \frac{q(s)}{\zeta(s)} = (\mathbf{M} \cdot s^2 + \mathbf{C} \cdot s + \mathbf{K})^{-1} \cdot (\mathbf{C}_\zeta \cdot s + \mathbf{K}_\zeta) \tag{6}$$

The operational transmittances for velocities and accelerations are expressed by relations (7) and (8), respectively:

$$H_{\dot{q}}(s) = \begin{bmatrix} H_{\dot{q}_1}(s) \\ H_{\dot{q}_2}(s) \end{bmatrix} = \frac{\dot{q}(s)}{\zeta(s)} = s \cdot H_q(s) \tag{7}$$

$$H_{\ddot{q}}(s) = \begin{bmatrix} H_{\ddot{q}_1}(s) \\ H_{\ddot{q}_2}(s) \end{bmatrix} = \frac{\ddot{q}(s)}{\zeta(s)} = s^2 \cdot H_q(s) \tag{8}$$

We can easily pass from the Laplace transform to the Fourier transform. The operational transmittances will then become spectral transmittances. In formal terms, this is expressed in passing from domain s to argument $i \cdot \omega$, by assuming the real part r of the expression $s = r + i \cdot \omega$ as zero. With such a substitution, the relations (4)-(8) still hold.

5. Random excitation from an uneven road surface

An assumption has been made here that the road surface is undeformable and is a realization of a stationary Gaussian random process. In the relevant ISO standard [8], a proposal has been made to classify road surfaces from A to H, i.e. from very good (A) through good (B), average (C), and poor (D) to very poor (E and further F, G, and H). The road of a specific class is described in the ISO standard [8] by the function of power spectral density (PSD) $S_d(\Omega)$ [m³/rad] of one longitudinal track parallel to the road centreline:

$$S_d(\Omega) = S_d(\Omega_0) \cdot (\Omega/\Omega_0)^{-w} \tag{9}$$

where:

$\Omega = 2\pi/L$ – angular frequency of the longitudinal road profile [rad/m];

L – road roughness wavelength [m];

Ω_0 – reference angular frequency [1/m] (in most cases, $\Omega0 = 1.0$);

$Sd(\Omega_0)$ – road roughness indicator [m³/rad], defining the general road surface condition (whether it is good or poor);

w – road waviness indicator [–], providing information whether long or short waves predominate in the road profile.

In the said ISO standard [8], roads of different classes differ from each other in the $Sd(\Omega_0)$ values. The exponent w has a constant value of $w = 2$. Fig. 3 shows power spectral density values of random road surface irregularities according to the ISO classification [8], in a log-log scale, for various forms of the independent variable.

The road roughness wavelength L values have been assumed as varying between 0.1 m and 100 m, which covers the "micro-profile" of road surface irregularities [9, 17, 18].
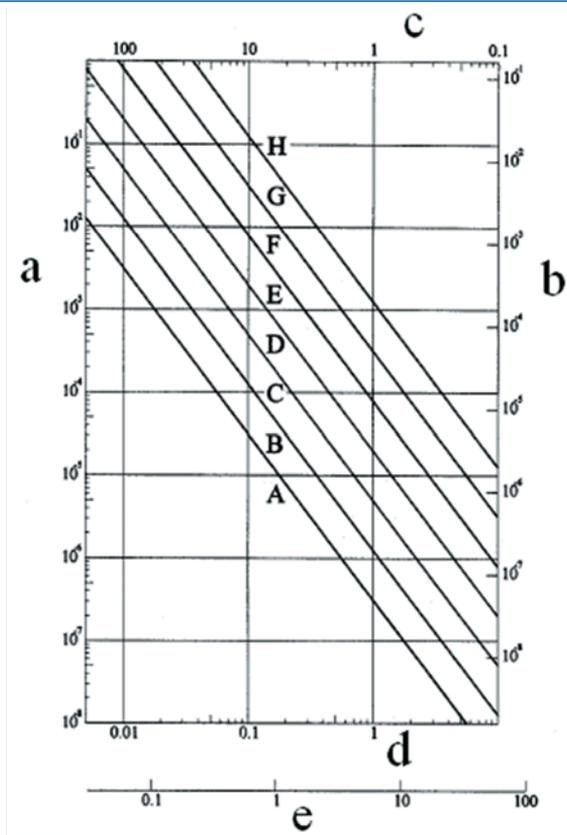
Fig. 3. Power spectral density values of random road surface irregularities according to the ISO classification [8]; road classes from A to H; log-log scale. Meaning of the lowercase letters in the drawing: a – power spectral density S_d **(1/L) [m³]; b – power spectral density** S_d **(Ω) [m³/rad]; c – wavelength** L **[m]; d – wave number 1/L [1/m]; e – angular frequency of the longitudinal road profile** $\Omega = 2\pi/L$ **[rad/m]**

6. Smoothing properties of vehicle tyres

In the pneumatic tyre model, the "one-point contact" model is usually used for the radial direction of vibrations [2, 3, 14, 15]. Therefore, the road roughness wavelength that is taken into account must be bounded from below. The smoothing properties of vehicle tyres may be taken into account by adopting a "fixed footprint tyre model" [2, 3, 14] (with averaging the road profile height over the tyre/road contact patch) and filtering the road roughness spectra. To do this, a filter was used with the absolute value of its transmittance being [14]:

$$\left| H_{op}(\Omega) \right| = \left| \sin(\Omega \cdot l_{op})/(\Omega \cdot l_{op}) \right| \tag{10}$$

where l_{op} [m] is a half of the length of the patch of contact between the tyre and the road surface assumed as being smooth and level, in static load conditions.

Fig. 4 represents the absolute value of the transmittance of a filter describing the smoothing properties of vehicle tyres, corresponding to the "constant patch model". Equation (11) shows a formal description of the said filtration, leading to determination of the power spectral density of road surface irregularities $S_{df}(\Omega)$ where the smoothing properties of vehicle tyres would be reflected:

$$S_{df}(\Omega) = \left| H_{op}(\Omega) \right|^2 S_d(\Omega) \tag{11}$$

The introduction of $S_{df}(\Omega)$ as an input makes it possible to use the one-point tyre/road contact model [2, 3, 14].
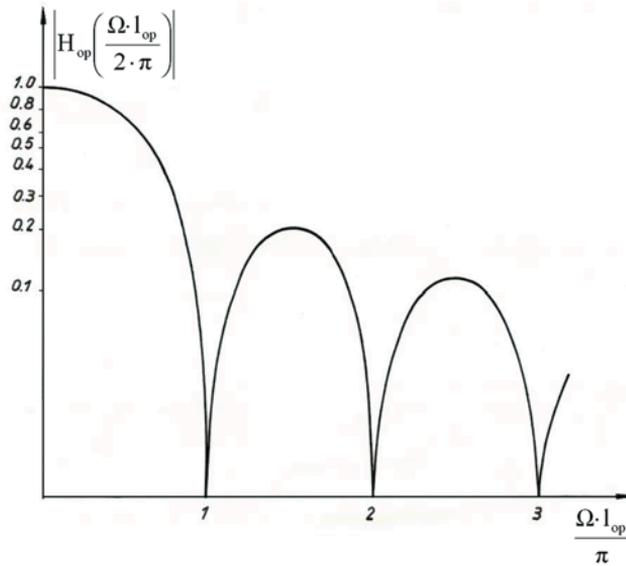
Fig. 4. Absolute value of the transmittance of a filter describing the smoothing properties of vehicle tyres, corresponding to the "constant patch model" [14] (for the notation used, see the text)

7. Automotive suspension damping selection criteria (optimization criteria)

As in publications [3, 4, 5, 6, 10, 11, 17, 18, 19, 25, 26, 27, 28, 29, 30, 31, 32], three criteria have been adopted to assess the correctness of selection of suspension damping coefficient c_l:

– minimization of the standard deviation of sprung mass acceleration, σ_a [m/s^2], which is a measure of vehicle occupants' discomfort;
– minimization of the standard deviation of the varying dynamic component (i.e. the dynamic value measured in relation to the static value) of the normal reaction at the tyre/road contact, σ_F [N], which is a measure of the safety hazard;

- reduction in the working displacements of the suspension system to a value lower than the suspension displacement limit r_{zg} [m].

In formal terms, these criteria may be described as follows (as a function of suspension damping coefficient c_1 and vehicle speed V):

$$Q(c_1, V) = w_a \cdot \sigma_a(c_1, V) + w_F \cdot \sigma_F(c_1, V) \quad \Rightarrow \text{minimum} \tag{12}$$

$$6 \cdot \sigma_{uz}(c_1, V) \leq r_{zg} \tag{13}$$

where:

$Q(c_1, V)$ [-] – the objective function subject to minimization;

w_a [1/m], w_F [1/N] – weighting factors for discomfort and safety hazard, respectively;

$\sigma_{uz}(c1, V)$ [m] – standard deviation of suspension deflection (measured in relation to the static value);

r_{zg} [m] – suspension displacement limit.

The above criteria are adopted for each of all the road surface quality classes taken into consideration. The factor "6" in formula (13) comes from the Gaussian distribution of the suspension deflection in the model under analysis. This stems from the known property of the response of a linear system to a Gaussian stationary excitation from road irregularities, as these irregularities have Gaussian distributions, too. The working displacement of the suspension system is treated here as a doubled value of the maximum dynamic deflection of the suspension system, which is equal to about $3 \cdot \sigma_{uz}$. The standard deviations σ_a, σ_F, and σ_{uz} are calculated from the following known formulas [1, 9, 10, 11, 16, 17, 18, 20, 21, 22, 23, 25, 32]:

$$\sigma_a = \sqrt{\int_0^{\omega_{max}} S_{\ddot{q}_1}(\omega) \cdot d\omega} = \sqrt{\int_0^{\omega_{max}} \left| H_{\ddot{q}_1}(i \cdot \omega) \right|^2 \cdot S_{df}(\omega) \cdot d\omega} \tag{14}$$

$$\sigma_F = \sqrt{\int_0^{\omega_{max}} S_F(\omega) \cdot d\omega} = \sqrt{\int_0^{\omega_{max}} \left| H_F(i \cdot \omega) \right|^2 \cdot S_{df}(\omega) \cdot d\omega} \tag{15}$$

$$\sigma_{uz} = \sqrt{\int_0^{\omega_{max}} S_{uz}(\omega) \cdot d\omega} = \sqrt{\int_0^{\omega_{max}} \left| H_{uz}(i \cdot \omega) \right|^2 \cdot S_{df}(\omega) \cdot d\omega} \tag{16}$$

where the new symbols are defined as follows:

$S_{\ddot{q}_1}(\omega), S_F(\omega), S_{uz}(\omega)$ – power spectral densities of sprung mass accelerations [m²/s³/rad], dynamic component of the normal reaction at the tyre/road contact [N²·s/rad], and suspension deflection [m²·s/rad], respectively;

$\omega = 2\pi \cdot f$ – radian frequency ω [rad/s] and Hertz frequency f [Hz];

$\omega_{max} = 2\pi \cdot f_{max}$ – maximum radian frequency ω_{max} [rad/s] and maximum Hertz frequency fmax [Hz] under consideration;

$H_{\ddot{q}_1}(i \cdot \omega)$ — spectral transmittance for the sprung mass acceleration (see 8) $[1/s^2]$;

$H_F(i \cdot \omega)$ — spectral transmittance for the dynamic component of the normal reaction at the tyre/road contact [N/m];

$H_{uz}(i \cdot \omega)$ — spectral transmittance for suspension deflection [-].

To pass from $S_{df}(\Omega)$ [m³/rad] to $S_{df}(\omega)$, i.e. to change the independent variable from Ω [rad/m] (angular frequency of the longitudinal road profile) to ω [rad/s] (radian frequency of the input vibration), Ω must be multiplied by the speed of vehicle motion v [m/s], with $S_{df}(\Omega)$ being simultaneously divided by v [m/s]. Thanks to this, the definite integrals of Sdf (Ω) and $S_{df}(\omega)$ in the mutually corresponding frequency bands under consideration will have the same value of the variance of road profile height ( ).

The Fourier transforms of the dynamic component of the normal reaction at the tyre/road contact and of the suspension deflection are defined by the following two equations, respectively:

$$F(i \cdot \omega) = c_2 \cdot [\dot{\xi}(i \cdot \omega) - \dot{z}_2(i \cdot \omega)] + k_2 \cdot [\xi(i \cdot \omega) - z_2(i \cdot \omega)] \qquad (17)$$

$$u_z(i \cdot \omega) = z_2(i \cdot \omega) - z_1(i \cdot \omega) \qquad (18)$$

Based on equations (6)-(8) as well as (17) and (18), after transformations, the following final concise forms of spectral transmittances have been obtained (with remembering that $q_1 = z_1$ and $q_2 = z_2$):

$$H_{\ddot{q}_1}(i \cdot \omega) = \frac{\ddot{q}_1(i \cdot \omega)}{\zeta(i \cdot \omega)} = -\omega^2 \cdot H_{q_1}(i \cdot \omega) \qquad (19)$$

$$H_F(i \cdot \omega) = \frac{F(i \cdot \omega)}{\zeta(i \cdot \omega)} = (i \cdot c_2 \cdot \omega + k_2) \cdot [1 - H_{q_2}(i \cdot \omega)] \qquad (20)$$

$$H_{uz}(i \cdot \omega) = \frac{q_2(i \cdot \omega) - q_1(i \cdot \omega)}{\zeta(i \cdot \omega)} = H_{q_2}(i \cdot \omega) - H_{q_1}(i \cdot \omega) \qquad (21)$$

8. Calculation data: parameters of the model and of the test conditions

The model parameters taken as an example corresponded to the data of the front suspension system of the Isuzu D-max motor vehicle: m_1 = 578 kg, m_2 = 69.5 kg, k_1 = 42 520 M/m, k_2 = 220 000 N/m, c_1 was changed in the calculations, and c_2 = 150 N·s/m. The length of the tyre/road contact patch in static conditions was $2 \cdot l_{op}$ = 0.185 m.

Three roads with the following values of the parameters defining the power spectral density of road surface irregularities were chosen for the calculations:

– road 1, of class B (good), $S_d(\Omega 0)$ = 0.000004 , Ω_0 = 1.0, w = 2;

–   road 2, of class C (average), $S_d(\Omega_0)$ = 0.000016 , Ω_0 = 1.0, w = 2;

–   road 3, of class D (poor), $S_d(\Omega_0)$ = 0.000064 , Ω_0 = 1.0, w = 2.

The lowest and highest road roughness wavelength values were L = 0.1 m and L = 100 m, respectively.

In consideration of the ISO standard provisions that concern the vibration comfort [7], the frequency band of 0-80 Hz (0-502.65 rad/s) was adopted for the analyses.

The analyses were carried out for 12 constant vehicle speeds V [km/h], changed within the range from 10 km/h to 120 km/h in steps of 10 km/h. The vehicle speed values expressed as v [m/s] and V [km/h] are connected with each other by the generally known relation v = V/3.6.

The damping coefficient c_1 [N·s/m] was changed and its values were indirectly expressed by means of a relative damping coefficient [1], i.e. by values γ [-] defined as follows:

$$\gamma = \frac{c_1}{c_{1kr}} = \frac{c_1}{2 \cdot m_1 \cdot \omega_{01}} = \frac{h}{\omega_{01}} \tag{22}$$

$$c_{1kr} = 2 \cdot m_1 \cdot \omega_{01} \tag{23}$$

$$h = c_1/2/m_1 \tag{24}$$

where:

c_{1kr} [N·s/m] – critical damping coefficient;

$\omega_{01} = 2 \cdot \pi \cdot f_{01}$ – the first (lower) natural radian frequency of the undamped system [rad/s];

f_{01} – the first (lower) natural Hertz frequency of the undamped system [Hz];

$$\omega_{01}^2 = \frac{k_1 \cdot m_2 + (k_1 + k_2) \cdot m_1}{2 \cdot m_1 \cdot m_2} - \sqrt{\left[\frac{k_1 \cdot m_2 + (k_1 + k_2) \cdot m_1}{2 \cdot m_1 \cdot m_2}\right]^2 - \frac{k_1 \cdot k_2}{m_1 \cdot m_2}} \tag{25}$$

The second (higher) natural radian frequency of the undamped system $\omega_{02} = 2 \cdot \pi \cdot f_{02}$ [rad/s] is defined by the following equation [1]:

$$\omega_{02}^2 = \frac{k_1 \cdot m_2 + (k_1 + k_2) \cdot m_1}{2 \cdot m_1 \cdot m_2} + \sqrt{\left[\frac{k_1 \cdot m_2 + (k_1 + k_2) \cdot m_1}{2 \cdot m_1 \cdot m_2}\right]^2 - \frac{k_1 \cdot k_2}{m_1 \cdot m_2}} \tag{26}$$

and f_{02} is the second (higher) natural Hertz frequency of the undamped system [Hz].

For the system under analysis, these values were ω_{01} = 7.839 rad/s, ω_{02} = 61.558 rad/s, f_{01} = 1.248 Hz, f_{02} = 9.797 Hz, c_{1kr} = 9 062 N·s/m.

The analyses were carried out for 26 values of the relative damping coefficient γ [-], changed within the range from 0.1 to 0.6 in steps of 0.02.

The value of the coefficient of damping in the suspension system was:

$$c_1 = \gamma \cdot c_{1kr} = \gamma \cdot 2 \cdot m_1 \cdot \omega_{01} \ [\text{N·s/m}] \tag{27}$$

The weighting factors for discomfort and safety hazard, w_a and w_F, were so selected that they reflected equal treatment of both of these criteria. Their values will be specified in a subsequent part of this study, after the stage of normalization of calculation results. The working displacements of the suspension systems were limited to a value of r_{zg} = 0.12 m, corresponding to the real linear range of operation of the suspension system of the vehicle under analysis. The parameters of the model and of the test conditions as described above have been brought together in Table 1.

Table 1. List of parameters of the model and of the test conditions

Item	Description	Symbol	Unit	Value
1.	Mass of the part of the vehicle body solid situated over the road wheel, "sprung mass"	m_1	kg	578
2.	Mass connected with the road wheel, "unsprung mass"	m_2	kg	69.5
3.	Suspension stiffness	k_1	N/m	42 520
4.	Radial stiffness of the road wheel	k_2	N/m	220 000
5.	Suspension damping coefficient	c_1	N·s/m	variable
6.	Radial damping coefficient of the pneumatic tyre	c_2	N·s/m	150
7.	Length of the tyre/road contact patch in static conditions	$2 \cdot l_{op}$	m	0.185
8.	Type (class) and power spectral density parameters of the first road chosen	Road 1: B (good)	–	–
		$S_d(\Omega_0)$	m³/rad	0.000004
		Ω_0	1/m	1.0
		w	–	2.0
9.	Type (class) and power spectral density parameters of the second road chosen	Road 2: C (average)	–	–
		$S_d(\Omega_0)$	m³/rad	0.000016
		Ω_0	1/m	1.0
		w	–	2.0
10.	Type (class) and power spectral density parameters of the third road chosen	Road 3: D (poor)	–	–
		$S_d(\Omega_0)$	m³/rad	0.000064
		Ω_0	1/m	1.0
		w	–	2.0

Table 1. List of parameters of the model and of the test conditions

Item	Description	Symbol	Unit	Value
11.	The lowest value of the road roughness wavelength	L_{min}	m	0.1
12.	The highest value of the road roughness wavelength	L_{max}	m	100.0
13.	The lowest Hertz (radian) frequency of the vibrations under analysis	f_{min} (ω_{min})	Hz (rad/s)	0 (0)
14.	The highest Hertz (radian) frequency of the vibrations under analysis	f_{max} (ω_{max})	Hz (rad/s)	80 (502.65)
15.	The first natural Hertz (radian) frequency of the undamped system	f_{01} (ω_{01})	Hz (rad/s)	1.248 (7.839)
16.	The second natural Hertz (radian) frequency of the undamped system	f_{02} (ω_{02})	Hz (rad/s)	9.797 (61.558)
17.	Critical suspension damping coefficient	c_{1kr}	N·s/m	9 062.0
18.	Vehicle speed range under analysis	V_{min}-V_{max} $(v_{min}$-$v_{max})$	km/h (m/s)	10.0-120.0 (2.78-33.33)
19.	Vehicle speed sampling step	ΔV (Δv)	km/h (m/s)	10.0 (2.78)
20.	The lowest value of the relative suspension damping coefficient	γ_{min}	–	0.1
21.	The highest value of the relative suspension damping coefficient	γ_{max}	–	0.6
22.	Sampling step of the relative suspension damping coefficient	$\Delta\gamma$	–	0.02
23.	Suspension displacement limit	r_{zg}	m	0.12

9. Calculation results before the modification of the optimization criteria

For the parameters of the model and of the test conditions as specified in Table 1, calculations were carried out in accordance with the algorithm presented in a previous part of this paper.

Figs. 5, 6, and 7 show the absolute values of spectral transmittances for sprung mass acceleration, for the dynamic component of the normal reaction at the tyre/road contact, and for suspension deflection, as functions of the excitation frequency, in the 0-80 Hz frequency band, for various values of the relative damping coefficient, ranging from 0.1 to 0.6. In each of the three drawings mentioned above, two maximums can be clearly seen for

frequencies close to the natural frequencies of the undamped system (1.248 Hz and 9.797 Hz), with the values of the maximums being the lower the higher the relative damping was. For the sprung mass acceleration (Fig. 5), the impact of damping was very high in the zone close to the first resonance, which was reflected in a drop in the absolute transmittance value with an increase in the damping. The influence of the damping is also visible in the inter-resonance and extra-resonance zones. In this case, an increase in the damping resulted in a growth in the absolute transmittance value, and to a significant extent (by 100-400 %) at that.

As regards the dynamic component of the normal reaction at the tyre/road contact (Fig. 6), an increase in the damping caused a reduction in the absolute transmittance value close to both resonance frequencies and a growth in this value in the inter-resonance zone (by even 400-500 % in this case); on the other hand, this impact was not so strong in the zone above the second resonance frequency, where the absolute transmittance values remained close to each other in spite of increasing frequencies.

The absolute value of the spectral transmittance of suspension deflection (Fig. 7) declined with increasing damping in the areas close to both resonances. In the inter-resonance and extra-resonance zones, this impact of the damping in the suspension system was quite small.
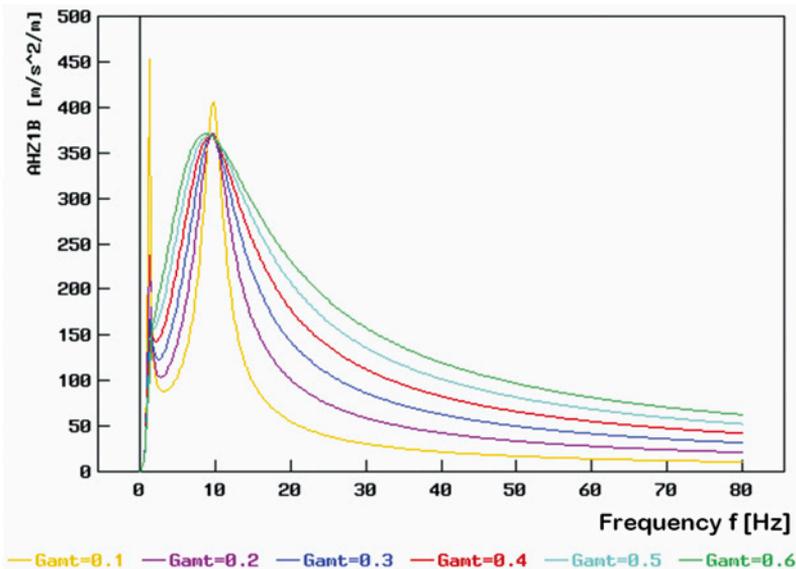
Fig. 5. Absolute value of the spectral transmittance for sprung mass acceleration (see (8) and (19), denoted by AHZ1B in the graph) vs. excitation frequency f, for various values of the relative damping coefficient (see (22), denoted by Gamt in the graph)
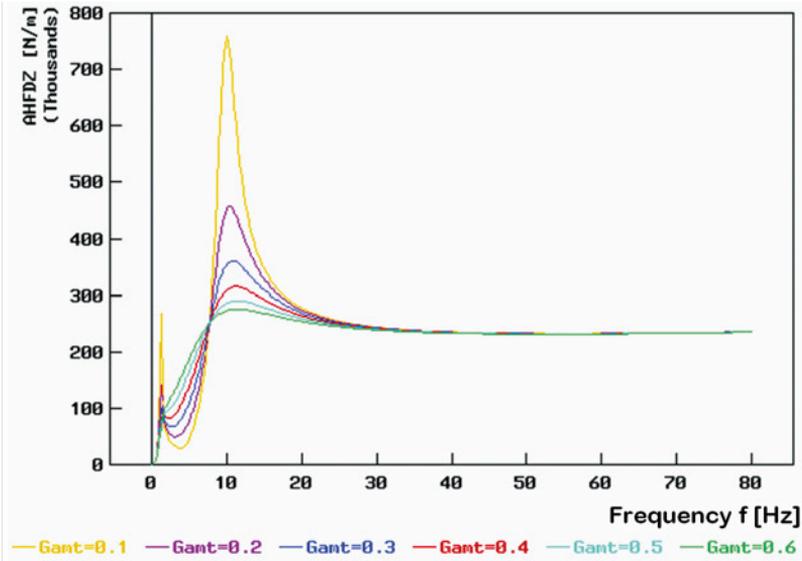
Fig. 6. Absolute value of the spectral transmittance for the dynamic component of the normal reaction at the tyre/road contact (see (17) and (20), denoted by AHFDZ in the graph) vs. excitation frequency f, for various values of the relative damping coefficient (see (22), denoted by Gamt in the graph)
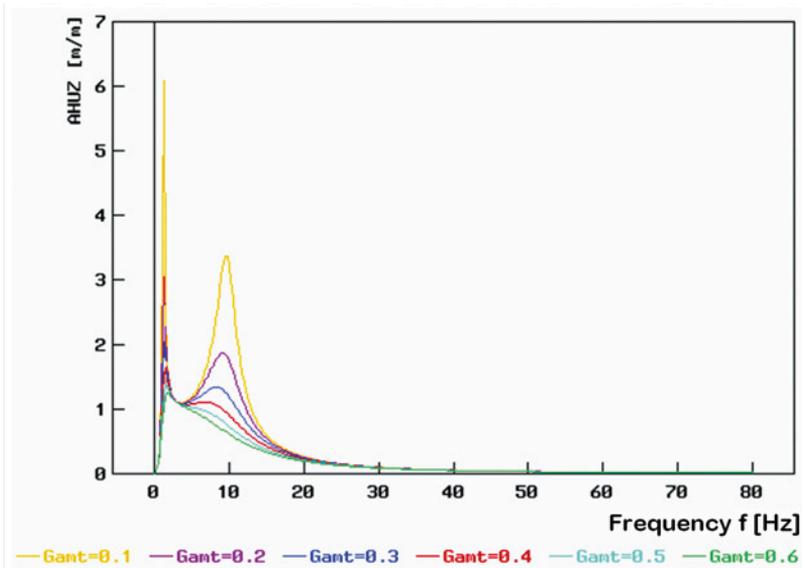
Fig. 7. Absolute value of the spectral transmittance for suspension deflection (see (18) and (21), denoted by AHUZ in the graph) vs. excitation frequency f, for various values of the relative damping coefficient (see (22), denoted by Gamt in the graph)

Fig. 8 shows (in a log-log scale) an example of power spectral density of road surface irregularities $S_d (\Omega)$ (see equation (9)) as a function of angular frequency of the longitudinal road profile Ω. The road under consideration in this example has been classified as a road of class C (i.e. of average quality), according to the relevant ISO standard [8]. An effect of filtration of this function, corresponding to the use of a "constant patch model" of the pneumatic tyre (see equations (10) and (11)), has also been presented. For angular frequencies exceeding 10 rad/m, the effect of taking into account the smoothing properties of the pneumatic tyre is very distinct, especially for the waves for which the ratio of the patch length to the wavelength is an integer. This is particularly clearly visible for $\Omega = 33.96$ rad/m, where $L = 2 \cdot l_p = 0.185$ m, i.e. the ratio of the patch length to the wavelength is equal to unity (see Fig. 4). The waves shorter than 0.1 m were disregarded, as mentioned in Section 8.
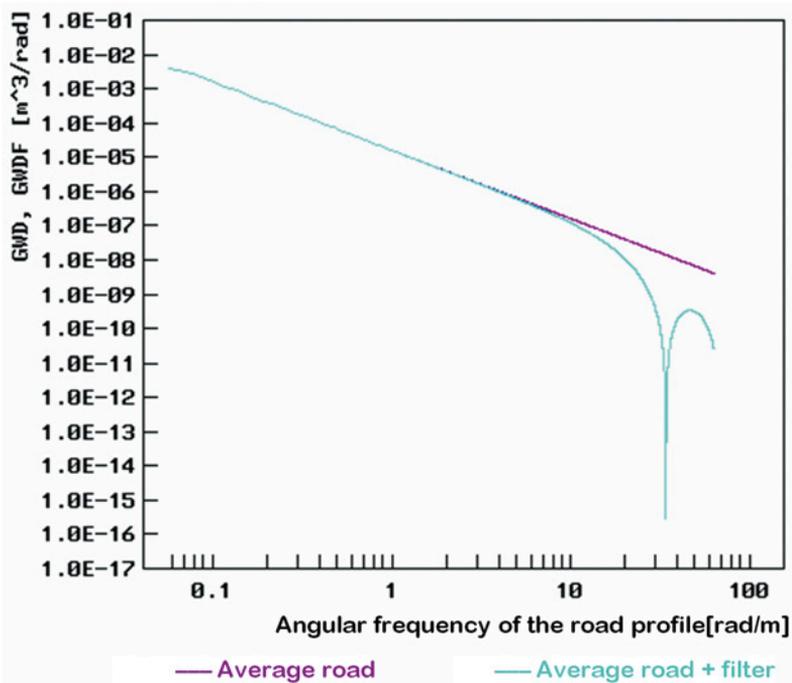
Fig. 8. Power spectral density of road surface irregularities (see (9), denoted by GWD in the graph, dark purple curve) and the effect of filtration (denoted by GWDF), obtained with the use of a "constant patch model" of the pneumatic tyre (aquamarine curve), vs. angular frequency of the road profile, for the road of class C (i.e. of average quality) according to the ISO standard [8]

Examples of power spectral density of road surface irregularities $S_{df}(\omega)$ for the road of class C (i.e. of average quality) according to the ISO standard [8] have been shown (in a log-log scale) in Fig. 9 as functions of the radian frequency ω [rad/s] for various vehicle speeds V [km/h]. The independent variable has been presented (after appropriate conversion) as excitation frequency f [Hz] for easier comparisons with other graphs included in this study. The effect of smoothing properties of the pneumatic tyre can be seen in the graphs, especially at high frequencies. This effect declined with increasing vehicle speeds because of growing excitation frequencies f [Hz] while the length of the tyre/road contact patch $2 \cdot l_p$ remained constant, with the frequencies considered being limited to a band of 0-80 Hz (see also Figs. 4 and 8 and equations (10) and (11)). At speeds of over 60 km/h, the influence of smoothing properties of the pneumatic tyre was already hardly noticeable.
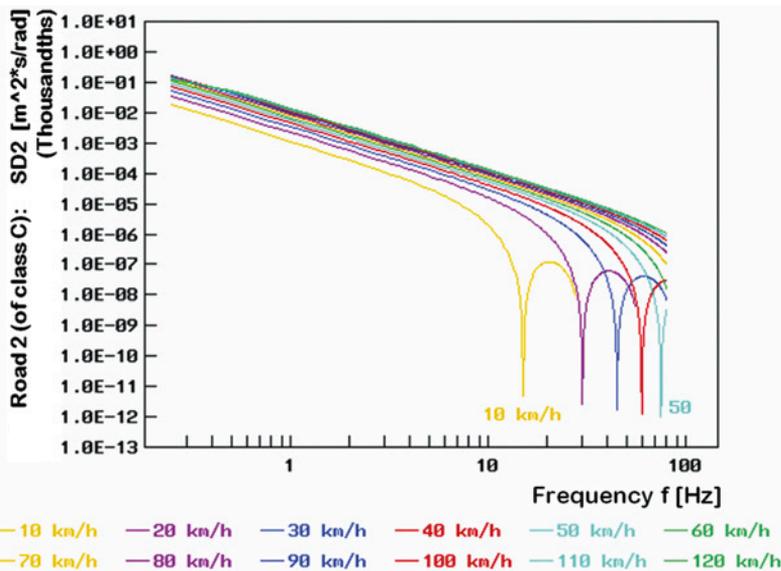
Fig. 9. Power spectral densities of road surface irregularities $S_{df}(\omega)$ **(denoted by SD2 in the graph) vs. the radian frequency** ω **[rad/s], presented as Hertz frequency** f **[Hz] of the excitation (for easier comparisons with other graphs), for the road of class C (i.e. of average quality) according to the ISO standard [8] and for various vehicle speeds** V **[km/h]**

Figs. 10, 11, and 12 show (in a log-log scale) power spectral densities as functions of excitation frequency f for the quantities that were taken as a basis for calculations of the criteria of assessment of the system under analysis. The road has been classified as a road of class C (i.e. of average quality), according to the relevant ISO standard [8]. The vehicle speed was V = 30 km/h. The graphs differ from each other in the values of the relative suspension damping coefficient (see (22)). Fig. 10 shows the power spectral densities of sprung mass accelerations (see the element of integration in equation (14)), Fig. 11 shows the power spectral densities of the dynamic component of the normal reaction at the tyre/road contact (see the element of integration in equation (15)), and Fig. 12 shows

the power spectral densities of suspension deflection (see the element of integration in equation (16)). The vehicle speed selected (30 km/h) was not very high so that the impact of the smoothing properties of pneumatic tyres could be observed at higher excitation frequencies (over 30 Hz in this case). This influence decreased with rising vehicle speed. The analogical results obtained for the other two roads (B and D) are similar in qualitative terms; they differ from each other in the values of the results obtained, which are lower for road B (of good quality) and higher for road D (of poor quality).

In all the three drawings mentioned above, a distinct impact of the relative damping and of the resonance frequencies of the undamped system (1.248 Hz and 9.797 Hz) on the shape of the curves plotted can be seen. For the sprung mass accelerations (Fig. 10), the impact of the damping was high for the first resonance (the damping reduced the power spectral density values) and in the inter-resonance and extra-resonance zones (where a growth in the damping caused the power spectral density to rise, and to a significant extend at that). For the dynamic component of the normal reaction at the tyre/road contact (Fig. 11), a growth in the damping reduced the power spectral density values in the resonance zones and in the extra-resonance zone, but this impact at frequencies exceeding that of the second resonance was insignificant. The values of the power spectral density of suspension deflection (Fig. 12) in the inter-resonance and extra-resonance zones only inconsiderably depended on the suspension damping; however, this impact can be seen in the resonance zones, where the damping reduced the power spectral density values.
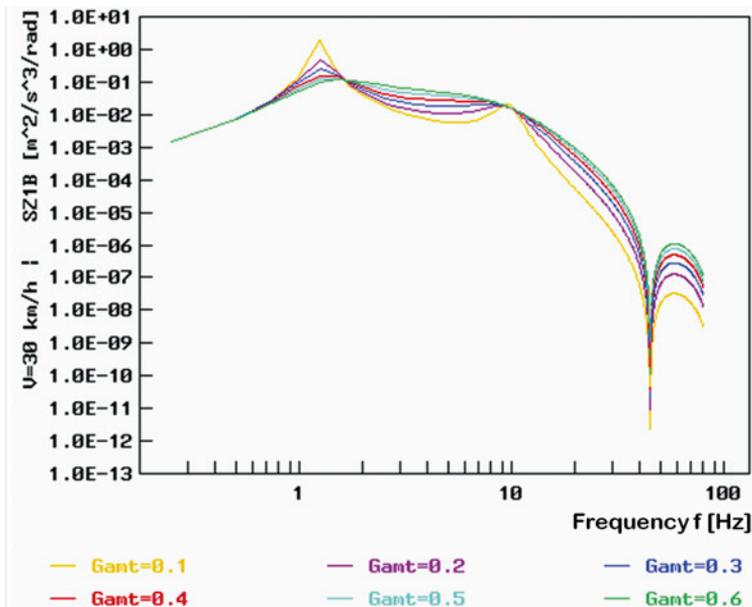
Fig. 10. Power spectral densities of sprung mass accelerations (denoted by SZ1B in the graph, see the element of integration in equation (14)) vs. excitation frequency f, for various values of the relative damping coefficient (see (22), denoted by Gamt in the graph), for the road of class C (i.e. of average quality) according to the ISO standard [8], and for a vehicle speed of $V = 30$ [km/h]
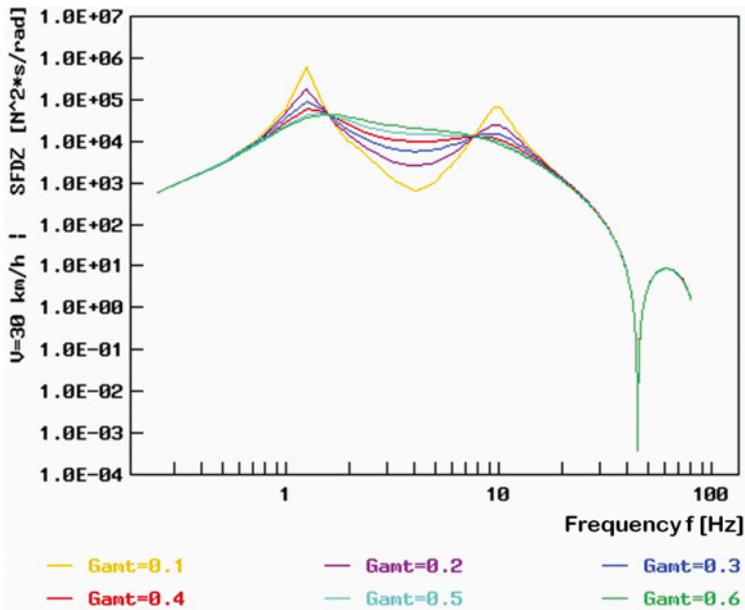
Fig. 11. Power spectral densities of the dynamic component of the normal reaction at the tyre/road contact (denoted by SFDZ in the graph, see the element of integration in equation (15)) vs. excitation frequency f, for various values of the relative damping coefficient (see (22), denoted by Gamt in the graph), for the road of class C (i.e. of average quality) according to the ISO standard [8], and for a vehicle speed of V = 30 [km/h]
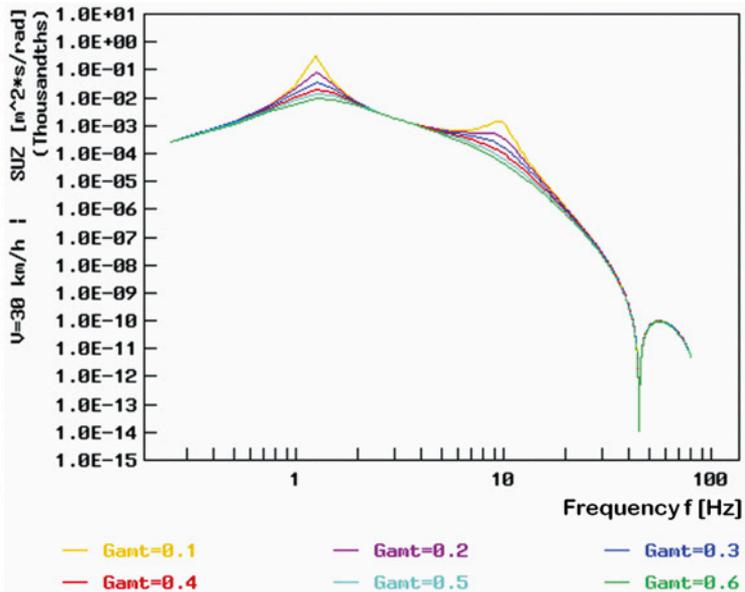
Fig. 12. Power spectral densities of suspension deflection (denoted by SUZ in the graph, see the element of integration in equation (16)) vs. excitation frequency f, for various values of the coefficient of relative damping (see (22), denoted by Gamt in the graph), for the road of class C (i.e. of average quality) according to the ISO standard [8], and for a vehicle speed of V = 30 [km/h]v

Standard deviations of the quantities taken as criteria of assessment of the system under analysis have been presented in Figs. 13, 14, and 15 as functions of the relative damping coefficient (see (22)), for the road of class C (i.e. of average quality) according to the ISO standard [8], and for 12 vehicle speed values ranging from 10 km/h to 120 km/h. Fig. 13 shows the standard deviations of sprung mass accelerations (see (14)), Fig. 14 shows the standard deviations of the dynamic component of the normal reaction at the tyre/road contact (see (15)), and Fig. 15 shows the standard deviations of suspension deflection (see (16)). The analogical results obtained for the other two roads (B and D) are similar in qualitative terms; they differ from each other in the values of the results obtained, but the locations of the minimums are also similar. The values of the results obtained are lower for road B (of good quality) and higher for road D (of poor quality).

The minimums of the standard deviations of sprung mass accelerations (see Fig. 13) occurred for the relative damping coefficient ranging from 0.25 to 0.30; with growing vehicle speed, they were slightly shifted towards the lower damping values. For the standard deviations of the dynamic component of the normal reaction at the tyre/road contact (see Fig. 14), the minimums corresponded to relative damping coefficient values of 0.35-0.40; for growing vehicle speed, they showed a slight trend towards the higher damping values.

In consideration of the above and of the shape of the curves in Figs. 13 and 14, a finding may be formulated that with increasing values of the relative damping coefficient, the measure of ride comfort grew better, but this was true only within the range of relative damping from zero to about 0.30; further growth in the relative damping coefficient resulted in worsening of the ride comfort. Additionally, when the relative damping coefficient grew from zero to about 0.40, the safety measure improved; however, this measure slightly decreased when the relative damping coefficient exceeded this threshold. This does not confirm the shapes of the qualitative curves shown in Fig. 1, especially the hypothesis that low damping is favourable for the measure of ride comfort and that high damping results in high safety. Thus, the author's doubts about the suggestions that the shapes of the curves shown in Fig. 1 may be interpreted not only in pictorial but also in qualitative and quantitative terms proved to be reasonable.

Fig. 15 clearly shows the existence of a monotonic trend towards lower suspension deflection values with increasing relative damping in the suspension. The intensity of this decrease, however, declines with growing values of the relative damping coefficient.

Among the optimization criteria proposed in Section 7, the one related to reduction in the working displacements of the suspension system (see (13)) can be most easily applied. The objective function $Q (c1)$ (see (12)) would create greater difficulties. Due to different measures of σ_a and σ_F, the weighting factors w_a and w_F cannot be dimensionless quantities. Therefore, it is more difficult to understand their sense. This was the first reason for modifying the form of the component elements of the objective function $Q (c_1)$. Another one was the will to refer to the comprehensibility of the relations presented in qualitative illustrations, such as that shown in Fig. 1.
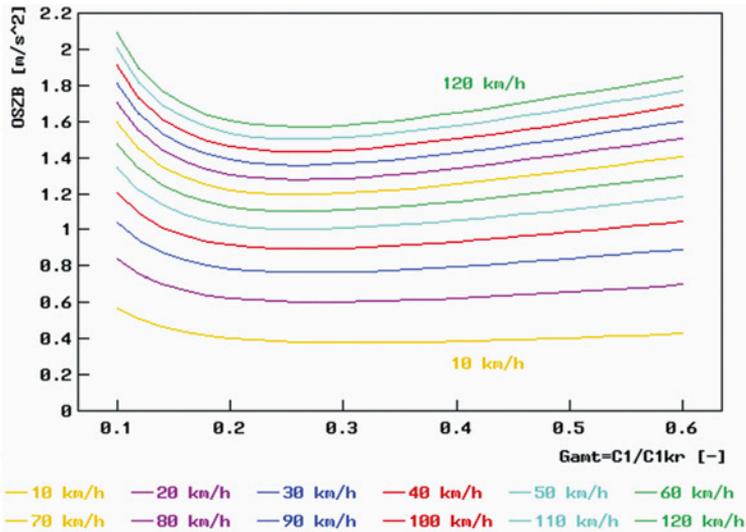
Fig. 13. Standard deviations of sprung mass accelerations (see (14), denoted by OSZB in the graph) vs. the relative damping coefficient (see (22), denoted by Gamt in the graph), for the road of class C (i.e. of average quality) according to the ISO standard [8] and for 12 vehicle speed values ranging from 10 km/h to 120 km/h
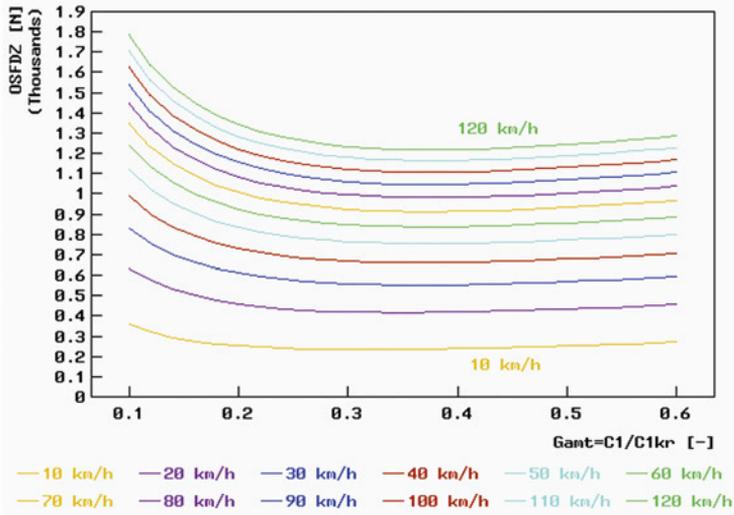
Fig. 14. Standard deviations of the dynamic component of the normal reaction at the tyre/road contact (see (15), denoted by OSFDZ in the graph) vs. the relative damping coefficient (see (22), denoted by Gamt in the graph), for the road of class C (i.e. of average quality) according to the ISO standard [8] and for 12 vehicle speed values ranging from 10 km/h to 120 km/h
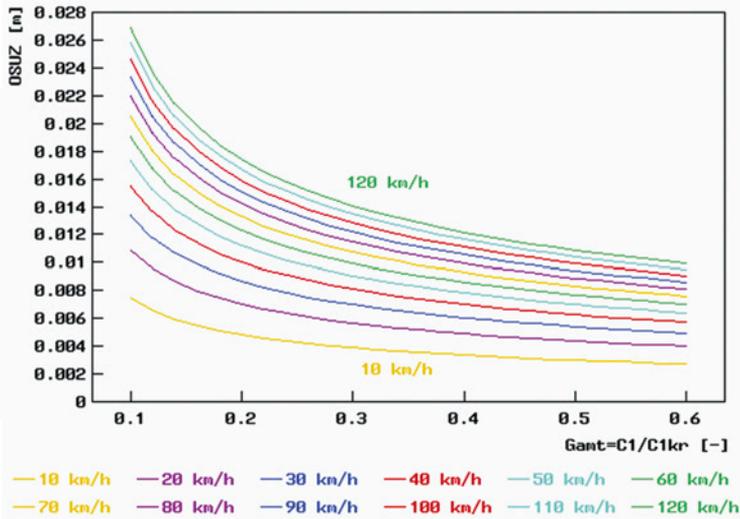
Fig. 15. **Standard deviations of suspension deflection (see (16), denoted by OSUZ in the graph) vs. the relative damping coefficient (see (22), denoted by Gamt in the graph), for the road of class C (i.e. of average quality) according to the ISO standard [8] and for 12 vehicle speed values ranging from 10 km/h to 120 km/h**

10. Modification of the optimization criteria

The modification process begins from normalization of the graphs presented in Figs. 13 and 14. The normalization is done by dividing each of the values in a curve (corresponding to individual vehicle speeds V) by the maximum value of the curve within the domain of c1. The symbol "max" has the meaning here as "the highest value" instead of a formal maximum.

$$\sigma_{au}(c_1, V) = 100\ \%\cdot\sigma_a(c_1, V)/\max\{\sigma_a(c_1, V)\}\ (\text{max. relative to } c_1, \text{ for a specific V value})\ (28)$$

$$\sigma_{Fu}(c_1, V) = 100\ \%\cdot\sigma_F(c_1, V)/\max\{\sigma_F(c_1, V)\}\ (\text{max. relative to } c_1, \text{ for a specific V value})\ (29)$$

Figs. 16 and 17 represent Figs. 13 and 14, respectively, after the normalization as described above. The higher the vehicle speeds V are, the closer the corresponding curves representing the normalized values are to each other. The minimums of the curves are better visible than they were before the normalization.
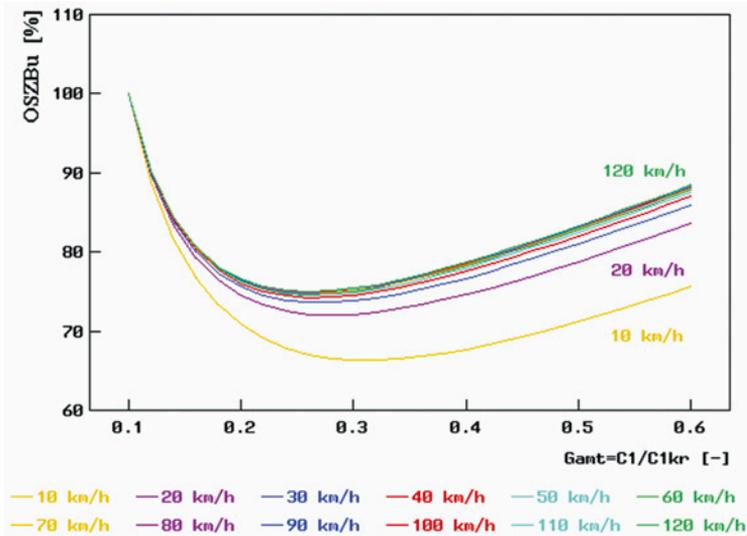
Fig. 16. Normalized standard deviations of sprung mass accelerations (see (28), denoted by OSZBu in the graph) vs. the relative damping coefficient (see (22), denoted by Gamt in the graph), for the road of class C (i.e. of average quality) according to the ISO standard [8] and for 12 vehicle speed values ranging from 10 km/h to 120 km/h
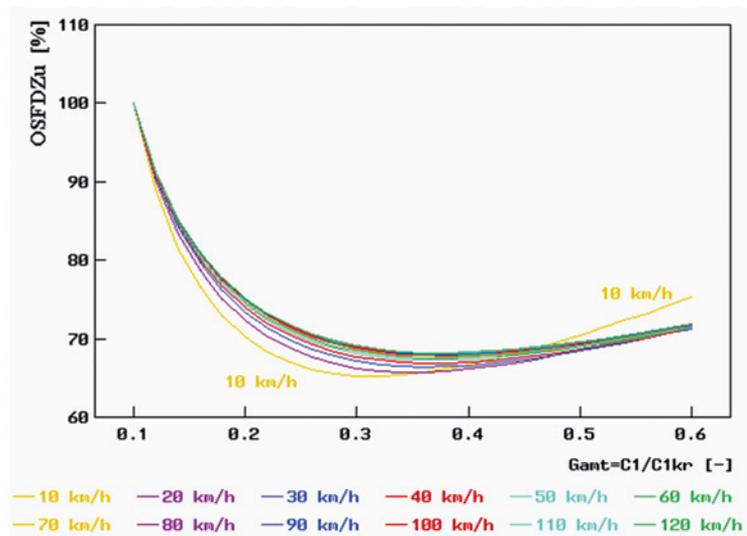
Fig. 17. Normalized standard deviations of the dynamic component of the normal reaction at the tyre/road contact (see (29), denoted by OSFDZu in the graph) vs. the relative damping coefficient (see (22), denoted by Gamt in the graph), for the road of class C (i.e. of average quality) according to the ISO standard [8] and for 12 vehicle speed values ranging from 10 km/h to 120 km/h

The next step in the modification process is changing the reference system, with maintaining the variability range from zero to 100 %, in order to show the quantities presented in such a way that 100 % would represent the maximum value. Thus, the comfort indicator WP1 and the safety indicator WP2 are determined. The symbol "min" has the meaning here of the formal minimum.

$$WP1\,(c_1) = -\sigma_{au}\,(c_1, V) + \min\,\{\sigma_{au}\,(c_1, V)\} + 100\,\% \text{ (min. relative to } c_1\text{, for all V values)} \quad (30)$$

$$WP2\,(c_1) = -\sigma_{Fu}\,(c_1, V) + \min\,\{\sigma_{Fu}\,(c_1, V)\} + 100\,\% \text{ (min. relative to } c_1\text{, for all V values)} \quad (31)$$

The modified criteria of assessing the correctness of selection of suspension damping coefficient c_1 (i.e. the criteria of optimizing the selection of suspension damping in respect of ride comfort and safety) have the following form:

$$Q_z\,(c_1) = w_k \cdot WP1\,(c_1) + w_b \cdot WP2\,(c_1) \quad \Rightarrow \text{maximum} \qquad (32)$$

$$6 \cdot \sigma_{uz}\,(c_1, V) \leq r_{zg} \qquad (33)$$

where the new symbols are defined as follows:

$Q_z\,(c_1)$ [%] – the modified objective function subject to maximization;

w_k [-], w_b [-] – weighting factors for comfort and safety, from within a range of ⟨0,1⟩;

WP1 [%],WP2 [%] – comfort and safety indicator (see relations (30) and (31));

r_{zg} [m] – suspension displacement limit.

Attention should be paid to a change in the terminology used: in place of the terms "discomfort" and "safety hazard" (see (12) and (13)), the notions "comfort indicator WP1" and "safety indicator WP2" (see (30) and (31) have now been introduced, because of their different monotonicity as functions of c_1. Now, the maximum of the new objective function $Q_z\,(c_1)$ is sought.

The next drawings present the comfort indicator WP1 (Fig. 18) and the safety indicator WP2 (Fig. 19) as functions of the relative damping, used as criteria of assessment of the system under analysis for the road of class C (i.e. of average quality) according to the ISO standard [8], and for 12 vehicle speed values ranging from 10 km/h to 120 km/h. The analogical results obtained for the other two roads (B and D) are similar in qualitative terms; they differ from each other in the values of the results obtained, but the locations of the maximums are also similar. The maximums of the comfort indicator WP1 (see Fig. 18) occurred for the relative damping coefficient ranging from 0.25 to 0.30; with growing vehicle speeds, they were shifted towards the lower damping values. For higher vehicle speeds, a decrease in the maximum values of the WP1 indicator can be seen as well. For the safety indicator WP2 (see Fig. 19), the maximums corresponded to relative damping coefficient values of 0.35-0.40; with growing vehicle speeds, they were shifted towards the higher damping values and the maximum values of the WP2 indicator slightly declined. The values of the comfort indicator WP1 and the safety indicator WP2 have been brought together in Fig. 20; this was possible thanks to their measures being identical. The curves presented correspond to those shown in Figs. 18 and 19, but they have been shown here for only four selected vehicle speeds, i.e. 30 km/h, 60 km/h, 90 km/h, and 120 km/h. When comparing Fig. 20 with the pictorial Fig. 1, we can easily show two areas where the graphs

are inconsistent with each other in qualitative terms. These areas have been marked with coloured ellipses. The comfort indicator WP1 (see the red ellipse) for the relative damping coefficient values in the interval ⟨0.1, 0.25⟩ is steeply decreasing with a decrease in the relative damping, while in Fig. 1, it reaches its highest value for the lowest damping. The safety indicator WP2 (see the green ellipse) for the interval ⟨0.4, 0.6⟩ of relative damping coefficient values gently declines with an increase in the relative damping, while in Fig. 1, it reaches its highest value for the highest damping. Therefore, Fig. 1 should be treated as a pictorial illustration only, which does not very accurately represent the properties of the system under analysis at that. For the relative damping coefficient of about 0.18, the WP1 and WP2 indicators assume equal values. The point of intersection of both curves, however, does not have the meaning of a Pareto-optimum, because both the WP1 and WP2 values are increasing with a growth in the damping (the point of intersection of the curves is situated before the maximums of both the WP1 and WP2 curves) and the related criterion of impossibility of improving one of the indicators (e.g. WP1) without worsening the other one (here WP2) (cf. [13, 33]) is not met.
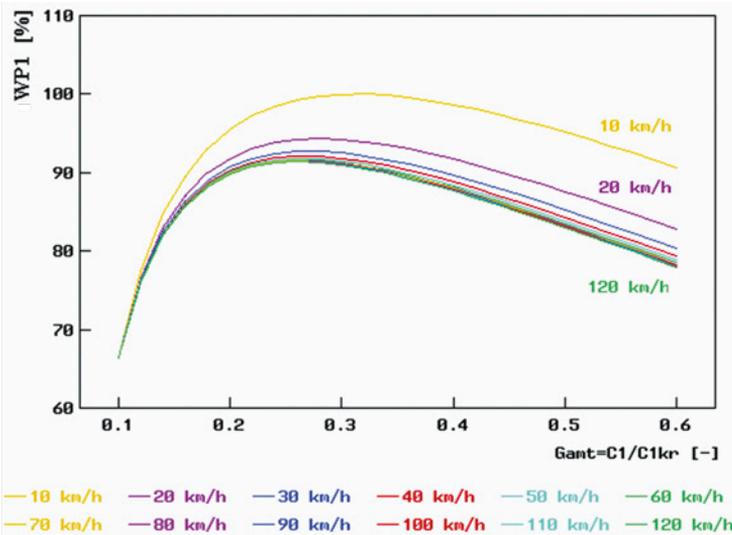
Fig. 18. Comfort indicator WP1 (see (30)) vs. the relative damping coefficient (see (22), denoted by Gamt in the graph), for the road of class C (i.e. of average quality) according to the ISO standard [8] and for 12 vehicle speed values ranging from 10 km/h to 120 km/h
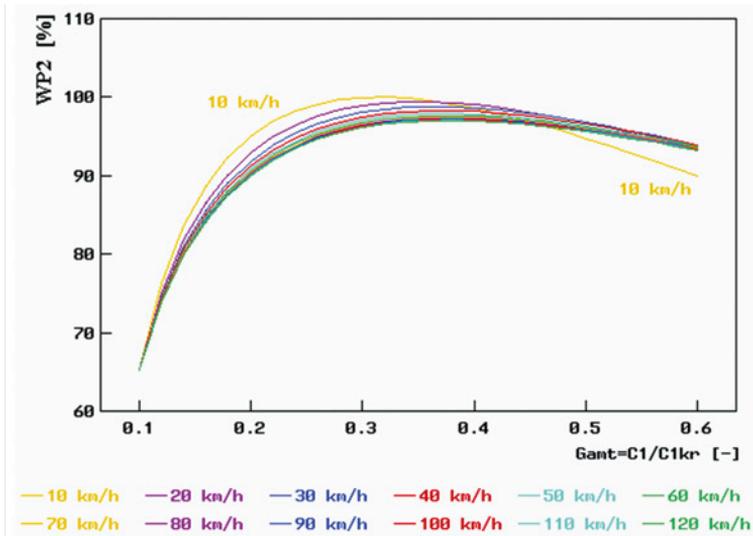
Fig. 19. Safety indicator WP2 (see (31)) vs. the relative damping coefficient (see (22), denoted by Gamt in the graph), for the road of class C (i.e. of average quality) according to the ISO standard [8] and for 12 vehicle speed values ranging from 10 km/h to 120 km/h
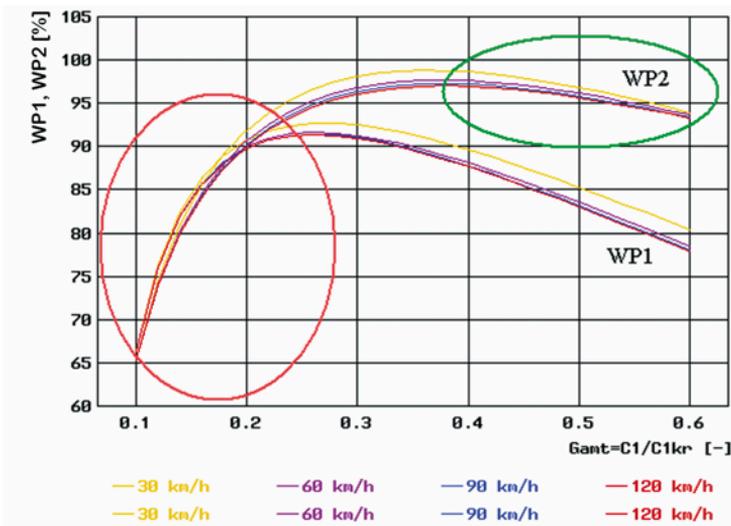
Fig. 20. Comfort indicator WP1 (see (30)) and safety indicator WP2 (see (31)) vs. the relative damping coefficient (see (22), denoted by Gamt in the graph), for the road of class C (i.e. of average quality) according to the ISO standard [8] and for 4 vehicle speed values ranging from 30 km/h to 120 km/h

11. Calculation results for the modified optimization criteria

Figs. 21 and 22 show the modified objective function $Q_z(c_1)$, calculated in accordance with equation (32), as a function of the relative damping coefficient (see (22)) for the road of class C (i.e. of average quality) according to the ISO standard [8], and for 3 vehicle speed values, i.e. 30 km/h, 90 km/h, and 90 km/h. The calculations were carried out for two sets of the weighting factors:

– set 1: $w_k = 0.5$ and $w_b = 0.5$;
– set 2: $w_k = 0.4$ and $w_b = 0.6$.

The curves denoted by "W:" in Figs. 21 and 22 have been plotted for set 2 of the weighting factors. Set 1 means equal treatment of comfort indicator WP1 and safety indicator WP2, while set 2 represents the case that safety is deemed 1.5 times as important as comfort (1.5 = 0.6/0.4).

Fig. 22 is a magnification of Fig. 21, with indication of the areas where the $Q_z(c_1)$ curves have their maximums. It can be seen that the optimum value of the relative damping coefficient γ for set 1 of the weighting factors is 0.31 (marked with the red ellipse in Fig. 22); for set 2, the optimum value of the relative damping coefficient γ is 0.32 (marked with the brown ellipse in Fig. 22). The optimum values of the suspension damping coefficient c_1 may be calculated from equation (27) with the use of the data given in Table 1:

– for set 1: $c_1 = 0.31 \cdot c_{1kr} = 0.31 \cdot 9\ 062$ N·s/m $\approx 2\ 810$ N·s/m
– for set 2: $c_1 = 0.32 \cdot c_{1kr} = 0.32 \cdot 9\ 062$ N·s/m $\approx 2\ 900$ N·s/m

The difference between the c_1 values is not too big, although the weighting factors adopted significantly differed from each other. The calculation results for the B and D road surface types have identical values, which can be explained by the linear form of the model used for the calculations and presented in Fig. 2.

A more complex situation is related to the third optimization criterion, i.e. the reduction in the working displacements of the suspension system (see equations (13) and (33)). It has been illustrated in Figs. 23a, 23b, and 23c. For the road of class B (i.e. of good quality, Fig. 23a), equations (13) and (33) are met for all the vehicle speed values under analysis and for the whole range of variability of the relative damping coefficient. For the road of class C (i.e. of average quality, Fig. 23b), equations (13) and (33) are met for all the vehicle speed values under analysis and for the relative damping coefficient higher than 0.159. For the road of class D (i.e. of poor quality, Fig. 23c), equations (13) and (33) are met for vehicle speed values not exceeding 60 km/h and for the relative damping coefficient higher than 0.30. In practice, it is hard to expect that any driver would decide to travel with a high speed on a road being in poor technical condition. Should it happen anyway, the suspension deflection would exceed the acceptable limit and this would mean the functioning of the suspension system in the range of operation of non-linear stroke limiters. Moreover, the probability of vehicle wheel lift-off would significantly increase. However, the phenomena of this kind are beyond the scope of applicability of the model used in this study. Hence, the limitation of the vehicle speed to 60 km/h on such a road is acceptable in this case.
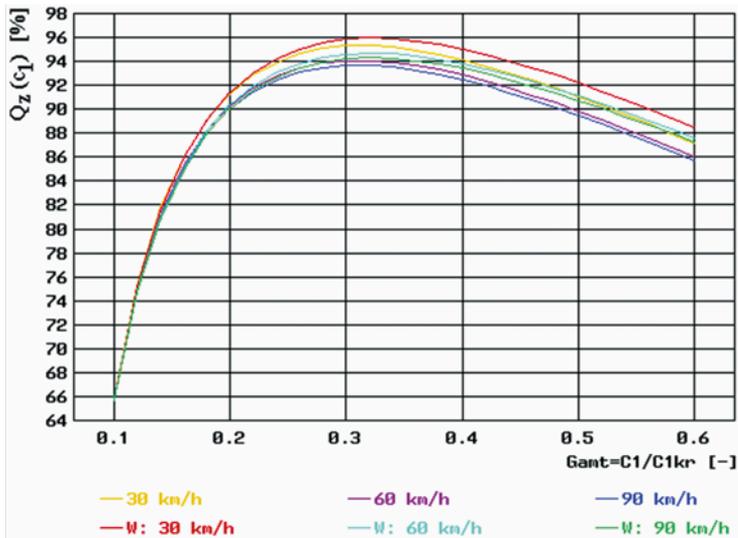
Fig. 21. Modified criterion $Q_z(c_1)$ of assessing the correctness of selection of suspension damping coefficient c1 (i.e. the criterion of optimizing the selection of suspension damping in respect of ride comfort and safety, see (32)) vs. the relative damping coefficient (see (22), denoted by Gamt in the graph), for the road of class C (i.e. of average quality) according to the ISO standard [8] and for 3 vehicle speed values, i.e. 30 km/h, 90 km/h, and 90 km/h (for the other symbols used, see the text)
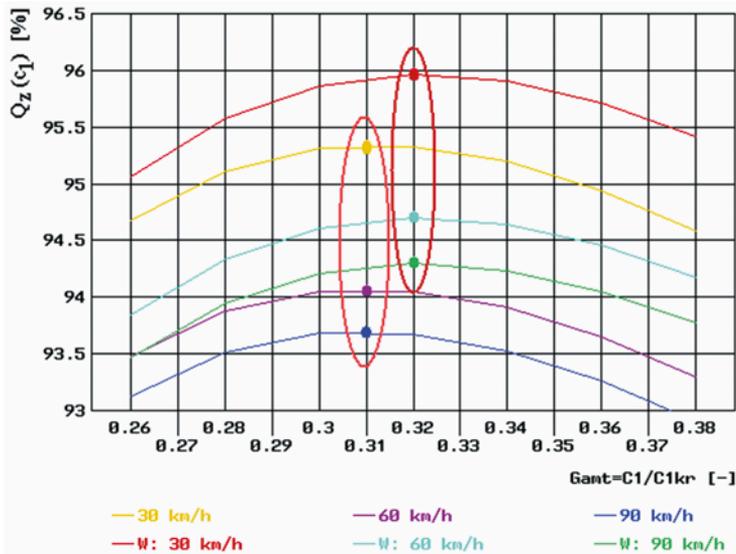
Fig. 22. Magnification of Fig. 21, with indication of the maximums of the curves shown. Modified criterion $Q_z(c_1)$ of assessing the correctness of selection of suspension damping coefficient c_1 (i.e. the criterion of optimizing the selection of suspension damping in respect of ride comfort and safety, see (32)) vs. the relative damping coefficient (see (22), denoted by Gamt in the graph), for the road of class C (i.e. of average quality) according to the ISO standard [8] and for 3 vehicle speed values, i.e. 30 km/h, 90 km/h, and 90 km/h (for the other symbols used, see the text)
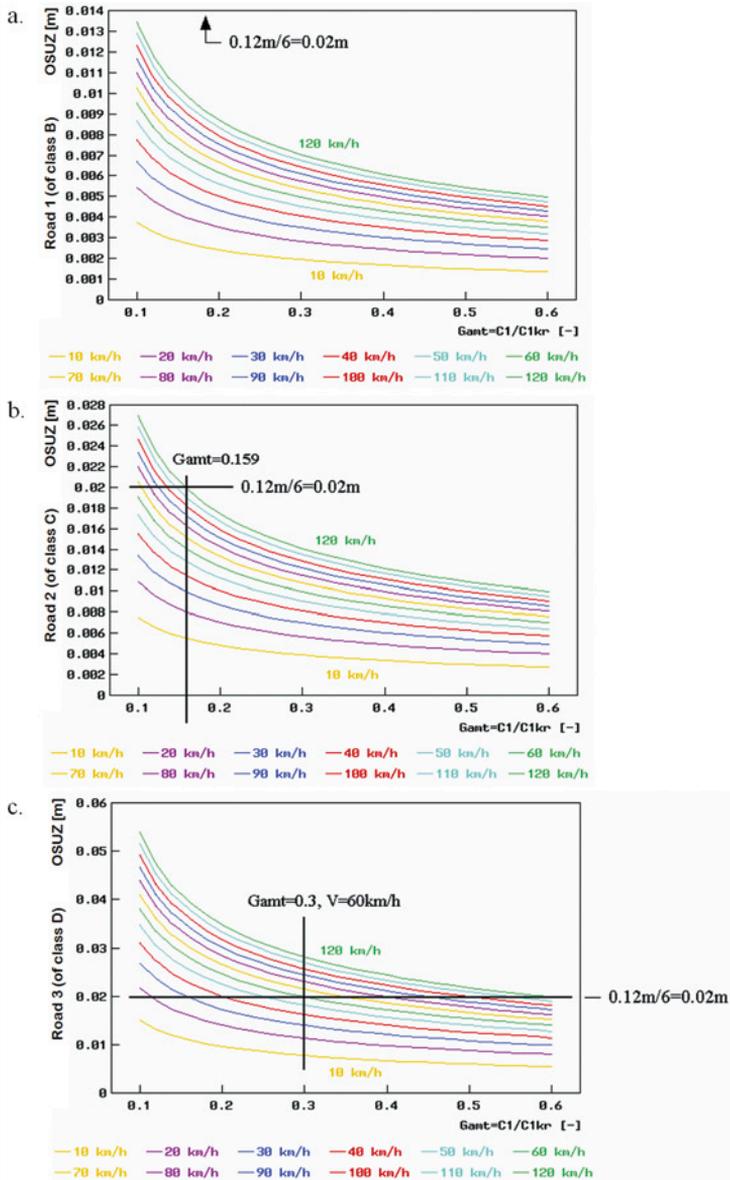
Fig. 23. Standard deviations of suspension deflection (see (16), denoted by OSUZ in the graphs) vs. the relative damping coefficient (see (22), denoted by Gamt in the graphs), for the roads of class B (i.e. of good quality, Fig. 23a), class C (i.e. of average quality, Fig. 23b), and class D (i.e. of poor quality, Fig. 23c), according to the ISO standard [8], and for 12 vehicle speed values ranging from 10 km/h to 120 km/h; the value of 0.12 m represents the suspension displacement limit adopted (r_{zg})

12. Conclusion

In this study, over 40-year achievements of many foreign and Polish authors in the field of methods of optimizing the characteristics of automotive suspension systems have been used. Results of calculations carried out within work dedicated to the optimization of linear damping in the passive suspension system of a vehicle moving on an uneven road surface with a random profile have been presented in detail. They have the form of a dimensionless objective function, which was adopted as a criterion of the optimization in respect of ride comfort and safety. The graphic form of this function, which is presented as a dependence on the dimensionless suspension damping coefficient, resembles the pictorial qualitative relationships, shown in many publications by other authors and facilitating the interpretation of final results of the optimization. The limitation of deflections of the suspension system has been taken into account, too.

The method presented is the first step in the process of optimizing the damping in automotive suspension systems. In further calculations, carried out with employing a quarter-car model, such issues as nonlinearities of spring characteristics of the suspension system and pneumatic tyres, asymmetry and nonlinearities of shock absorber characteristics, dry friction in the suspension system, and wheel lift-off should be taken into account. The next step should include the use of three-dimensional vehicle motion models, which most accurately reflect the properties of a real vehicle.

Information/Acknowledgements

The full text of the Article is available in Polish online on the website http://archiwummotoryzacji.pl.

Tekst artykułu w polskiej wersji językowej dostępny jest na stronie http://archiwummotoryzacji.pl.

References

[1]   Arczyński S. Mechanika ruchu samochodu. Warszawa: WNT; 1993.

[2]   Captain K M, Boghani A B, Wormley D N. Analytical tire models for dynamic vehicle simulation. Vehicle System Dynamics. 1979; 8(1): 1-32.

[3]   Crolla D A. Vehicle dynamics – theory into practice. Journal of Automobile Engineering. 1996; 210(2): 83-94.

[4] Firth G R. The performance of vehicle suspensions fitted with controllable dampers [dissertation]. The University of Leeds, Department of Mechanical Engineering; 1991.

[5] Gobbi M, Levi F, Mastinu G. Multi-objective stochastic optimization of the suspension system of road vehicles. Journal of Sound and Vibration. 2006; 298: 1055-1072.

[6] Gobbi M, Mastinu G. Analytical description and optimization of the dynamic behaviour of passively suspended vehicles. Journal of Sound and Vibration. 2001; 245(3): 457-481.

[7] ISO 2631–1:1985 and 1997: Mechanical vibration and shock – Evaluation of human exposure to whole-body vibration – Part 1: General Requirements. International Organization for Standardization.

[8] ISO 8608:1995: Mechanical vibration – Road surface profiles – Reporting of measured data. International Organization for Standardization.

[9] Kamiński E, Pokorski J. Teoria samochodu. Dynamika zawieszeń i układów napędowych pojazdów samochodowych. Warszawa: WKŁ; 1983.

[10] Kasprzyk T, Prochowski L, Szurkowski Z. Optymalizacja własności sprężystych i dobór konstrukcji ogumienia samochodu osobowego dla różnych warunków eksploatacji. Technika Motoryzacyjna. 1974; Part I: 10: 10-12; Part II: 11: 14-19.

[11] Kasprzyk T, Prochowski L. Teoria samochodu. Obciążenia dynamiczne zawieszeń. Warszawa: WKŁ; 1990.

[12] Konieczny J. Laboratory tests of active suspension system. Journal of KONES Powertrain and Transport. 2011; 18(1): 263-272.

[13] Kwarciński T. Sprawiedliwość czy efektywność? Analiza wykorzystująca ekonometryczny model wzrostu gospodarczego z historycznie optymalnym zróżnicowaniem. Acta Universitatis Lodziensis. Folia Oeconomica. 2007 [cited 23 Oct 2015]; 213: 109-124. Available from: http://kwarcinski.ovh.org/do_pobrania/artykuly/sprawiedliwosc_efektywnosc.pdf

[14] Lozia Z. Wybrane zagadnienia symulacji cyfrowej procesu hamowania samochodu dwuosiowego na nierównej nawierzchni drogi [dissertation]. Warsaw University of Technology, Faculty of Automotive and Construction Machinery Engineering: 1985.

[15] Lozia Z. Analiza ruchu samochodu dwuosiowego na tle modelowania jego dynamiki. Prace Naukowe Politechniki Warszawskiej. Transport. 1998; 41: 3-175.

[16] Meirovitch L. Elements of vibration analysis. United States: McGraw-Hill Kogakusha. 1975. 495 p.

[17] Mitschke M. Teoria samochodu. Dynamika samochodu. Warszawa: WKŁ; 1977.

[18] Mitschke M. Dynamika samochodu: drgania. Warszawa: WKŁ; 1989.

[19] Muluka V. Optimal suspension damping and axle vibration absorber for reduction of dynamic tire loads [dissertation]. Concordia University, Department of Mechanical Engineering, Montreal, Quebec, Canada: 1998.

[20] Newland D E. An introduction to random vibrations and spectral analysis. United States: Longman; 1984. 478 p.

[21] Osiecki J. Podstawy analizy drgań mechanicznych. Kielce: Kielce University of Technology; 1979.

[22] Osiecki J. Dynamika maszyn. Warszawa: Military University of Technology; 1994.

[23] Osiecki J, Gromadowski T, Stępiński B. Badania pojazdów samochodowych i ich zespołów na symulacyjnych stanowiskach badawczych. Radom: Wydawnictwo Instytutu Technologii Eksploatacji–PIB; 2006. 226 p.

[24] Patil S A, Joshi S G. Experimental analysis of 2 DOF quarter-car passive and hydraulic active suspension systems for ride comfort. Systems Science & Control Engineering: An Open Access Journal. 2014; 2(1): 621-631.

[25] Rotenberg R W. Zawieszenie samochodu. Warszawa: WKŁ; 1974.

[26] Ryba D. Improvements of dynamic characteristics of automobile suspension systems. Part I. Two-mass systems. Vehicle System Dynamics. 1974; 3(1): 17-46.

[27] Sekulić D, Devidović V. The effect of stiffness and damping of the suspension system elements on the optimization of the vibrational behavior of a bus. International Journal for Traffic and Transport Engineering. 2011; 1(4): 231-244.

[28] Sharp R S. Crolla D A. Road vehicle suspension system design – a review. Vehicle System Dynamics. 1987; 16: 167-192.

[29] Sharp R S, Hassan S A. An evaluation of passive automotive suspension systems with variable stiffness and damping parameters. Vehicle System Dynamice. 1986; 15: 335-350.

[30] Ślaski G. Studium projektowania zawieszeń samochodowych o zmiennym tłumieniu [dissertation]. Poznan University of Technology; 2012.

[31] Verros G, Natsiavas S, Papadimitriou C. Design optimization of quarter-car models with passive and semi-active suspensions under random excitation. Journal of Vibration and Control. 2005; 11: 581-606.

[32] Wong, J Y. Theory of ground vehicles. Canada: John Wiley & Sons; 2001.

[33] Encyklopedia PWN [cited 22 Oct 2015]. Available from: http://encyklopedia.pwn.pl/haslo/optimum-w-sensie-Pareto;3951452.html.